

Article

Testing Joints between Walls Made of AAC Masonry Units

Radosław Jasiński¹ and Iwona Galman^{2*}

¹ Department of Building Structures, Silesian University of Technology, Akademicka 5, 44-100 Gliwice, Poland, radoslaw.jasinski@polsl.pl, ORCID: 0000-0003-4015-4971 (R.J.)

² Department of Structural Engineering, Silesian University of Technology, Akademicka 5, 44-100 Gliwice, Poland, iwona.galman@polsl.pl, ORCID: 0000-0002-0196-6478 (I.G.)

* Correspondence: iwona.galman@polsl.pl; Tel. +48 32 237 22 88

Abstract: Joints between walls are very important for structural analysis of each masonry building at the global and local level. This issue was often neglected in case of traditional joints and relatively squat walls. Nowadays the issue of wall joints is becoming particularly important due to the continuous strive for simplifying structures, introducing new technologies and materials. Eurocode 6 and other standards (USA, Canadian, Chinese, and Japanese) recommend inspecting joints between walls, but no detail procedures have been specified. This paper presents our own tests on joints between walls made of autoclaved aerated concrete (AAC) masonry units. Tests included reference models composed of two wall panels joined perpendicularly with a masonry bond (6 models), traditional steel and modified connectors (12 models). A shape and size of test models and structure of a test stand were determined on the basis of the analysis of the current knowledge, pilot studies and numerical analyses of FEM. The analysis referred to the morphology and failure mechanism of models. Load-displacement relationships for different types of joints were compared and obtained results were referred to results for reference models. A mechanism of cracking and failure was found to vary, and clear differences in behaviour and load capacity of each type of joints were observed. Individual working phases of joints were determined and defined, and the empirical approach was suggested to determine forces and displacement of wall joints.

Keywords: masonry structures; stiffening walls; wall joints; connectors; bed joint reinforcement

1. Introduction

The review of tests on joints described in the paper [1] showed the lack of comprehensive papers on the behaviour of wall joints. That did not only refer to walls made of AAC masonry units, but also made of other masonry units. A poor insight into the issue of joints and the mutual action of walls resulted in neglecting calculations for such structures. Design standards lack guidelines for determining internal forces and stresses acting on wall intersections, and for determining conditions to verify ULS and SLS conditions. Few tests are insufficient to describe the mechanism of joints, much less to develop guidelines for designing and constructing. Moreover, there is a need to design a connector in a new shape to satisfy demands of the market which is aimed at optimizing existing solutions. A new connector should meet requirements of ultimate states and simultaneously should have a simple construction, easy assembly and much higher performance reliability at the phase after achieving the greatest loading. Therefore, overall aims of own tests were specified and they included:

- determination of the cracking and failure mechanisms of joints between AAC walls,
- comparison of load capacity of wall joints using traditional masonry bonds and steel connectors,
- optimization of the shape of a steel connector.

Moreover, authors made an attempt to build simplified models representing the behaviour of reinforced and unreinforced joints, which was described in this paper and the paper [2]. Tests and analyses presented in this paper were completed with new series of tests.

2. Programme of own tests

Three series (12 test models in total) in the same shape and dimensions were prepared and tested. Models of T shape were monosymmetric, with the web and flange length of ~89 cm. A vertical joint, whose structure varied intentionally, was formed between loaded and unloaded walls. A series of research models marked with **P** had traditional masonry joints between the web and the flange (Fig. 1a). Those elements were regarded as reference models, whose mechanical parameters and behaviour at loading and failure were compared with results from other tests. In two other series, joints between webs and flanges were made with steel connectors (wall geometry acc. to Fig. 1b). They were single punched flat bars in series **B10** (Fig. 1c), and modified flat bars with a broadened central part in series **BP10** (Fig. 1d). That solution was proposed on the basis of own tests [2] on perforated connectors. Broadening of the central part was intended to increase flexural capacity of the connector and its stiffness. The proposed shape is copyrighted on the basis of an application to the Polish Patent Office [15]. Joints made of galvanized perforated steel with a thickness of 1 mm were used in both series.

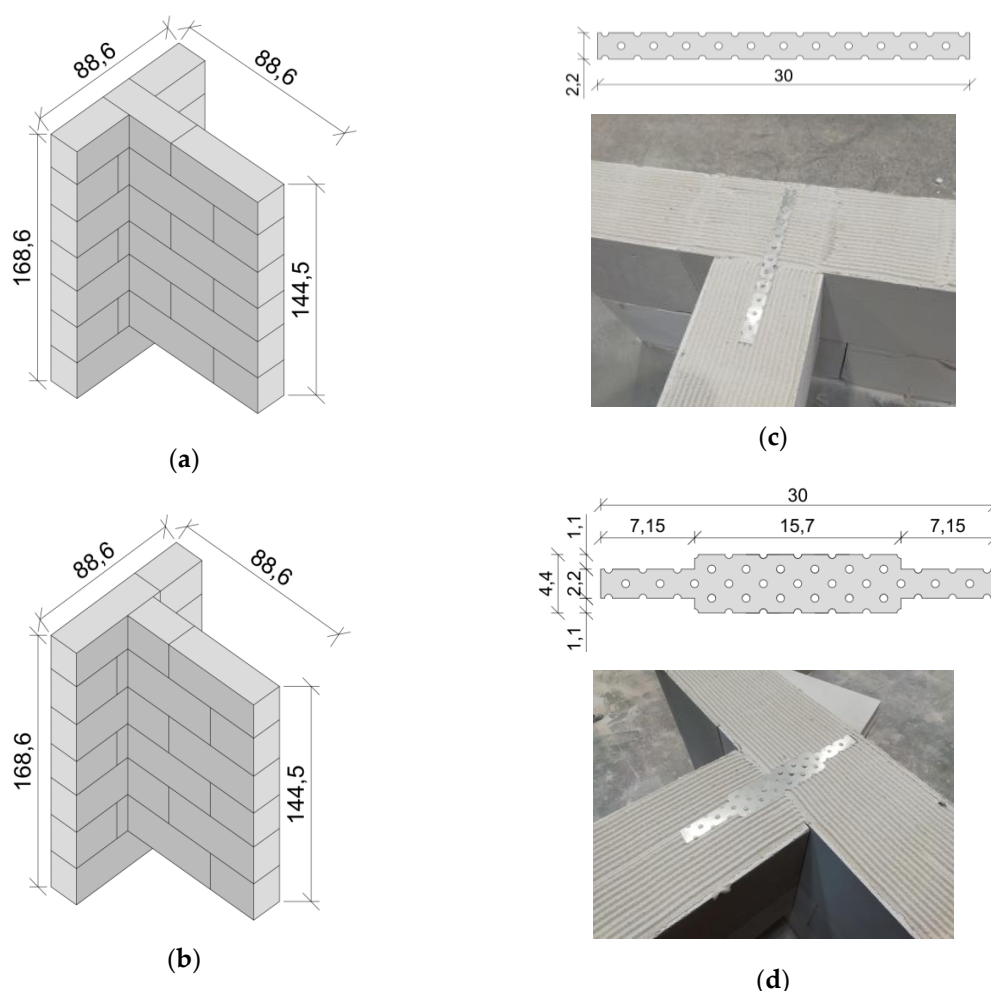


Figure 1. Geometry and details of research models and: a) traditional masonry bond, P series, b) walls with steel joints (B10 and BP10 series), c) joining method with a punched flat bar, d) joining method with a punched broadened flat bar [cm]

Tests were conducted in a test stand specially designed for that purpose – Fig. 2. Models 1a and 1b with confining elements 3 and elements taking load 2 were put on the strong floor (panel 1b) and

placed on a dynamometer 6, which with a resistor 4 was acting as a fixed articulated support. Models were placed below a steel frame 8, to which a hydraulic actuator was fixed (an operating capacity of 1000 kN) generating shearing at a constant displacement gain equal to 1mm/min. The structure response was registered using an inductive force transducer with an operating capacity of 250 kN and reading accuracy of ± 2.5 kN. Prestress of 0.1 MPa was exerted using reinforced concrete elements 3 and steel strands 7 to model considerable length of a joined wall in panel 1b. Models were loaded during one cycle until their destruction. Vertical load generating shear was transmitted linearly along the whole height of the wall through elements 2. As a result, shear stresses in joints was distributed uniformly. Loading and displacement of a loaded wall against the unloaded one were continually registered during tests. Two independent types of software were used to register data. One side of the research model was monitored using ARAMIS - an optical sensor of displacements. And another side was monitored with inductive transducers of displacement of type PJX-10 and an operating capacity of 10 mm and the accuracy of ± 0.002 mm.

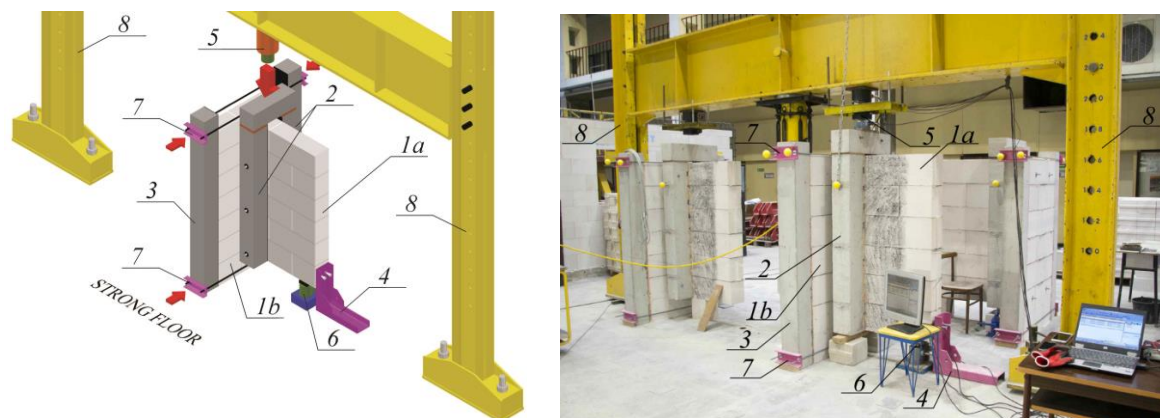


Figure 2. A scheme and photo of a test stand: 1a - longitudinal wall, 1b - transverse wall, 2 - reinforced concrete column transferring shear load, 3 - reinforced concrete pillars limiting horizontal deformation, 4 - horizontal support, 5 - system of the hydraulic cylinder and the force gauge used to induce shear stress, 6 - force gauge, vertical reaction, 7 - horizontal tie, 8 - steel frame

Tests were performed on models made of AAC masonry units with system mortar for thin joints and unfilled head joints. Compressive strength of masonry specified in PN-EN 1052-1:2000 [3]) and presented in the paper [4] was $f_c = 2.97$ N/mm², and the modulus of elasticity was $E_m = 2040$ N/mm². The initial shear value determined according to PN-EN 1052-3:2004 [5] and presented in the paper [6] was $f_{vo} = 0.31$ N/mm². An average friction coefficient in joints without mortar was $\mu = 0.92$ [10]. The shear modulus determined according to ASTM E519-81 [7] and presented in the paper [8] was $G = 329$ N/mm². Additional tests on steel connectors – Fig. 3 were conducted according to the standard [13]. Three elements were chosen randomly from each series of connectors and placed in jaws of a testing machine. Basic mechanical parameters of connectors were determined by controlling the displacement gain. Measurement of strains was non-contact with a video-extensometer MEVIX 200. Strain was measured using a base with the length $L_e = 53.5$ mm in standard connectors and $L_e = 75.0$ mm in thickened connectors. Fig. 3 illustrates σ – ε relationships. Stress-strain relationship of tested connectors was found to have no clear yield point. Therefore, results were approximated with a two-linear relationship. A symbolic yield point f_y was determined at the intersection of straight lines. The slope of the tangent straight line presented within the range of 0 – f_y was assumed as the average, initial modulus of elasticity E_s . Tensile strength was determined at failure of specimens, and tangent of straight line slope within the range of f_y – f_t was determined as the average secant modulus of elasticity E_t . Test results for connectors and the research programme are compared in Table 1.

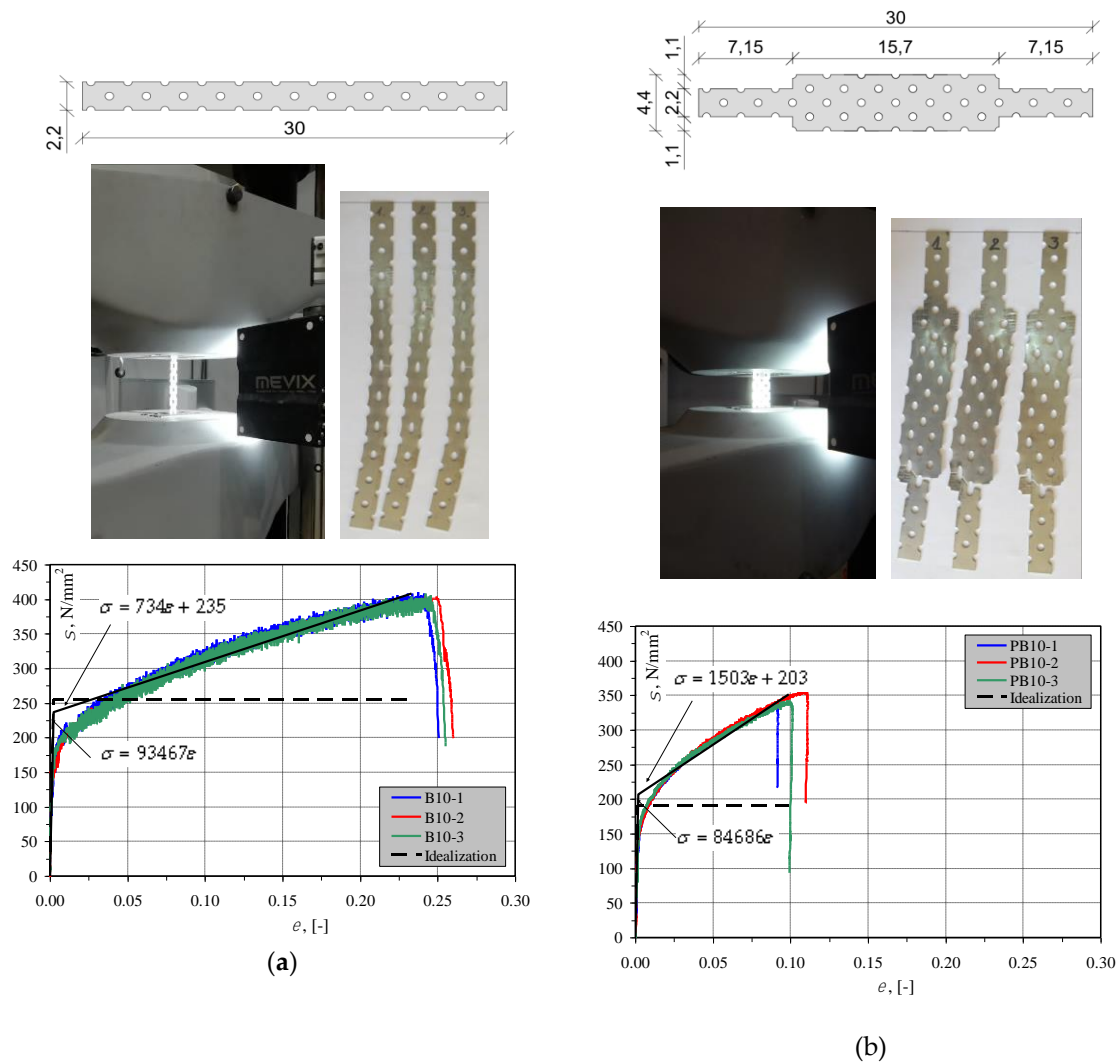


Figure 3. Testing connectors: a) connectors B10, b) connectors BP10

Table 1. Programme of tests and basic characteristics of connectors

Name of series	Type of joint	A mm ²	I mm ⁴	f_y/f_t N/mm ²	E_s/E_t N/mm ²	Number of models
P	Traditional masonry bond	--	--	--	--	6
B10	Punched steel flat bar $b \times t = 22 \times 1$ mm	22	1.83	236/408	93467/743	3
BP10	Punched broadened flat bar $b \times t = 44 \times 1$ mm	44	3.67	207/345	84686/1503	3

A – area of gross section, I – moment of inertia of gross section, f_y – average yield stress, f_t – tensile strength, E_s – average initial modulus of elasticity, E_t – average secant modulus of elasticity

3. Test results and their analysis

3.1. Unreinforced models

The behaviour of all unreinforced models was similar. No cracking noise and no visible splitting on lateral surfaces of elements were noticed at the initial phase of loading. Non-dilatation strain in some parts of the wall was observed. That phase lasted until the appearance of first diagonal cracks in the adjacent vicinity of wall joints – Figs 4a and 4b. Load increments caused a distinct development of cracks present at the place of joint and the propagation towards the reinforced concrete pole which transferred loading (Fig. 4c). The greatest force was registered at that working phase. Continued loading led to a distinct growth of mutual displacements and the rotation of joined walls. The joint was removed after the destruction – Fig. 4d. Almost vertical shearing of elements forming the bond was found. No clear damage was reported in case of other elements.

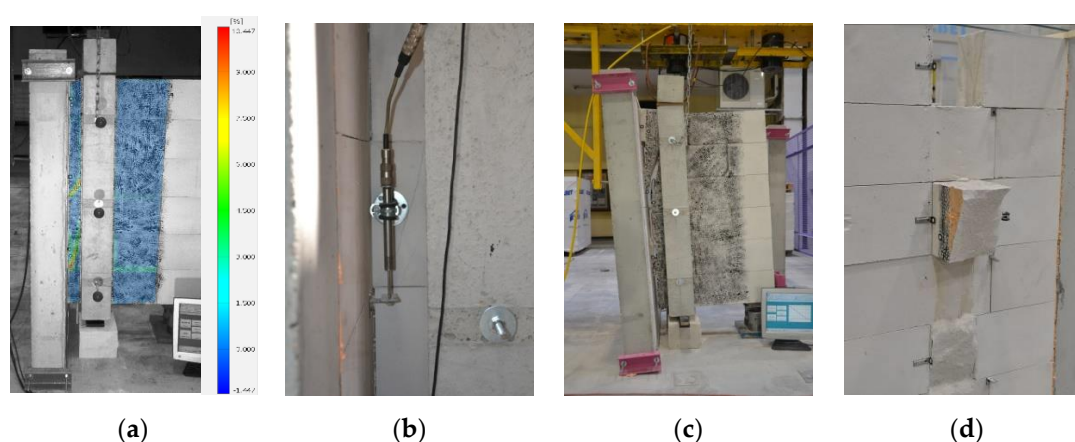


Figure 4. Destruction of models of series P a) a first crack on the reference model P_2 b) a first crack on the reference model P_6 c) joint after failure P_5 c) joint after failure P_3

The cracking mechanism for elements is also visible on diagrams illustrating the relationship between the load N and relative (mutual) displacement u of bonded walls – Fig. 5. Until cracking of the contact surface observed under the load $N_{cr} = 27.3 - 54.1$ kN, increments in relative displacements u were almost directly proportional, thus that working phase of the joint was called the elastic phase. After cracking at the post-elastic phase, stiffness was reduced, however joints still had the capacity for taking the load.

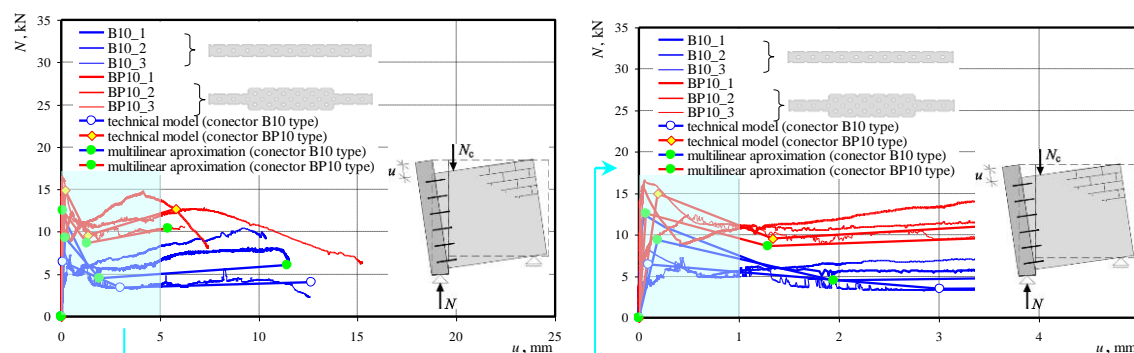


Figure 5. Relationship between the total force and average displacement for test results and calculations

That phase was completed at maximum force values within the range $N_u = 38.6 - 59.8$ kN. Continued attempts of loading at the failure phase resulted in a clear drop in values of forces

registered by a dynamometer, and an increment in relative displacements. Force were close to 0, and the joint had a capacity of taking some load. At that working phase of joint, forces were called aggregate interlocking forces having the value of $N_{ag} = 14.1 - 31.1$ kN. Further increment in joint displacements caused a minor load increase - the reinforcement. The last registered forces called residual forces preceded the failure that resulted in total splitting of bonded elements and the mutual rotation. Their value ranged within $N_r = 8.4 - 42.9$ kN. Forces and corresponding displacements are presented in Tables 2 and 3, and the linear approximation of results is shown in Fig. 6. Joint stiffness was determined at each working phase according to equations (1) – (3) and they are presented in Table 4:

joint stiffness at the elastic phase

$$K_t = \frac{N_{cr}}{u_{cr}}, \quad (1)$$

joint stiffness at the post-elastic phase

$$K_p = \frac{N_u - N_{cr}}{u_u - u_{cr}}, \quad (2)$$

joint stiffness at the failure phase

$$K_r = \frac{|N_r - N_u|}{u_r - u_u}. \quad (3)$$

Table 2. Test results for joints between unreinforced walls

Model	Force at the time of cracking		Maximum force		Aggregate interlocking force		Residual force	
	$N_{cr,i}$	$N_{cr,mv}$	$N_{u,i}$	$N_{u,mv}$	N_{ag}	$N_{ag,mv,i}$	$N_{r,i}$	$N_{r,mv}$
	kN	kN	kN	kN	kN	kN	kN	kN
P_1	27.3		56.3		31.1		20.7	
P_2	42.6		50.0		14.7		10.2	
P_3	31.2	39.2	38.6	50.7	25.5	24.9	13.8	16.2
P_4	54.1		59.8		--		8.36	
P_5	35.1		48.1		--		--	
P_6	45.1		51.6		28.264		27.9	

Table 3. Test results for joints between unreinforced walls - displacements

Model	Displacement at the time of cracking		Displacement right before failure		Displacement at aggregate interlocking force		Residual displacement	
	$u_{cr,i}$	$u_{cr,mv}$	$u_{u,i}$	$u_{u,mv}$	$u_{ag,i}$	$u_{ag,mv}$	$u_{r,i}$	$u_{r,mv}$
	mm	mm	mm	mm	mm	mm	mm	mm
P_1	0.07		0.31		2.43		6.36	
P_2	0.12		0.25		1.95		6.97	
P_3	0.12	0.09	0.16	0.23	2.22	2.08	5.64	5.58
P_4	0.07		0.17		--		6.72	
P_5	0.06		0.10		--		--	
P_6	0.08		0.36		1.71		2.22	

Table 4. Test results for joints between unreinforced walls - joint stiffness

Model	Elastic joint stiffness		Post-elastic joint stiffness		Residual joint stiffness	
	$K_{t,i}$	$K_{t,mv}$	$K_{p,i}$	$K_{p,mv}$	$K_{r,i}$	$K_{r,mv}$
	MN/m	MN/m	MN/m	MN/m	MN/m	MN/m
P_1	413	496	119	123	5.89	7.39
P_2	341		60		5.93	
P_3	268		163		4.51	
P_4	804		52.8		7.86	
P_5	562		322		--	
P_6	590		23		12.75	

3.1.1. Validation of the model with unreinforced wall joints

Performed tests were used to generalize the obtained results by proposing the so called standard model. The following assumptions were made:

- a non-linear relationship $N - u$ determined from tests could be replaced with a multi-sectional relationship expressing all observed working phases:
 - the elastic phase observed in the load range $0 - N_{cr}$,
 - the post-elastic phase observed in the load range $N_{cr} - N_u$,
 - the failure phase observed in the load range $N_u - N_{ag} - N_r$
- all material parameters used in the model were suggested to be specified in standard and normalised methods,
- the model would be subjected to statistical validation on the basis of performed tests.

The following empirical relationships were recommended to determine forces and displacements in individual working phases:

Forces and displacements at the elastic phase:

$$N_{cr} = \alpha_1 \tau_{cr,RL} A, \quad (4)$$

$$u_{cr} = N_{cr} / K_t = N_{cr} / \alpha K_{RL} \quad (5)$$

Forces and displacements at the post-elastic phase:

$$N_u = \beta_1 \tau_{u,RL} A, \quad (6)$$

$$u_u = u_{cr} + (N_u - N_{cr}) / K_p = u_{cr} + (N_u - N_{cr}) / \beta K_t, \quad (7)$$

where: $A = 0.26 \text{ m}^2$ – joint area, $\alpha, \alpha_1, \beta, \beta_1$ – empirical coefficients.

Shear parameters determined during tests on diagonal compression performed in compliance with ASTM E519-81 were $\tau_{cr,RL} = 0.192 \text{ MPa}$, $\tau_{u,RL} = 0.196 \text{ N/mm}^2$ and stiffness $K_{RL} = 117.1 \text{ MN/m}$ were used as reference values in above equations. At the beginning of the failure phase, residual and aggregate interlocking forces were determined from the following equations:

$$N_r = \gamma \tau_{u,RL} A, \quad (8)$$

$$N_{ag} = \gamma_1 \tau_{u,RL} A, \quad (9)$$

where: γ, γ_1 – empirical coefficients.

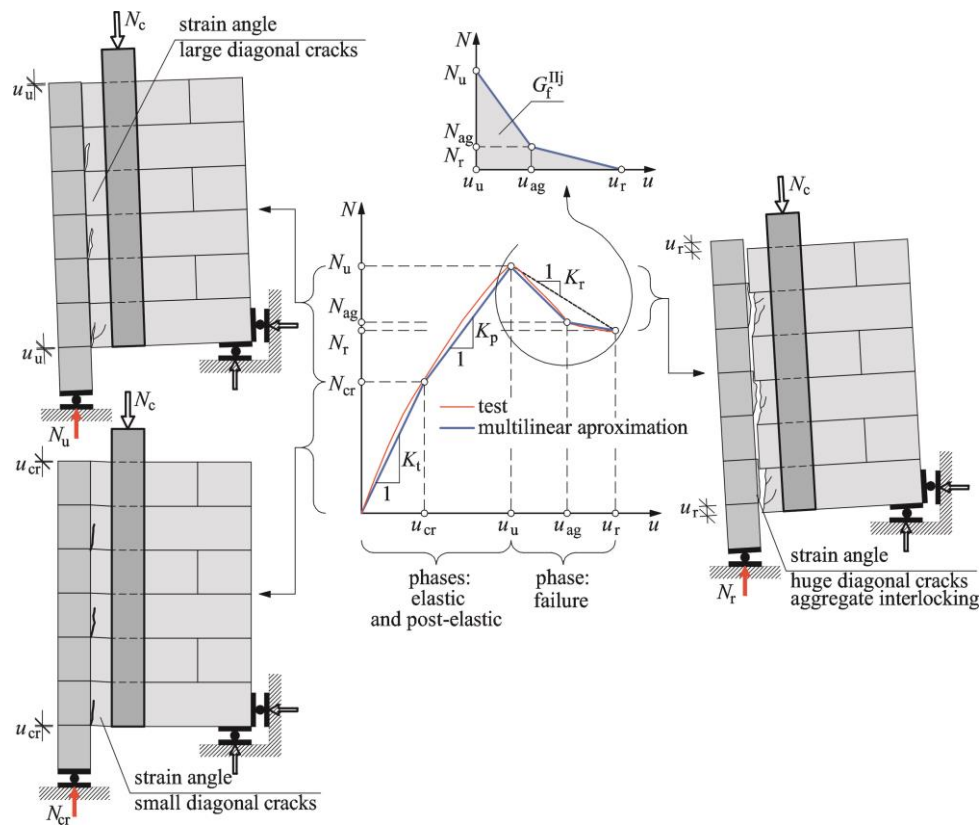


Figure 6. Approximation of work of unreinforced joint between masonry walls

Displacements corresponding to the aggregate interlocking force were determined from the following empirical relationship:

$$u_{ag} = \omega \tau_{u,RL} / K_{RL} , \quad (10)$$

where: ω – empirical coefficients.

Values of empirical coefficients were calculated using results from material tests and test on individual elements. Also, boundary values of average coefficients α , α_1 , β , β_1 , γ , γ_1 and ω were determined at the significance level $\alpha = 0.8$ for creating the reference model [14]. As the sample size was small $n < 30$, the following relationship was used:

$$P\left(\bar{x} - t_{1-\alpha/2} \frac{S}{\sqrt{n}} < m < \bar{x} + t_{1-\alpha/2} \frac{S}{\sqrt{n}}\right) = 1 - \alpha , \quad (11)$$

where: $\bar{x} = \sqrt{\sum(x-x)/n}$ – the mean value of the random sample, $S = \sqrt{\sum(x-x)^2/(n-1)}$ – standard deviation of the sample, $t_{1-\alpha/2}$ – statistics with the Student's t-distribution and $n-1$ degrees of freedom.

Lower and upper values from the confidence interval of average coefficients are presented in Table 5.

Table 5. Validation of empirical coefficient of the model with unreinforced wall joints

Model	x_i						
	$\alpha_i = \frac{K_{t,i}}{K_{RL}}$	$\beta_i = \frac{K_{p,i}}{K_{t,i}}$	$\alpha_{1,i} = \frac{N_{cr,i}}{\tau_{cr,RL}A}$	$\beta_{1,i} = \frac{N_{u,i}}{\tau_{u,RL}A}$	$\gamma_i = \frac{N_{r,i}}{\tau_{u,RL}A}$	$\gamma_{1,i} = \frac{N_{ag,i}}{\tau_{u,RL}A}$	$\omega_i = \frac{u_{ag,i}K_{RL}}{\tau_{u,RL}A}$
P_1	3.51	0.29	0.55	1.10	0.4	0.6	5.61
P_2	2.90	0.17	0.85	0.98	0.2	0.3	4.49
P_3	2.27	0.61	0.62	0.76	0.3	0.5	5.13
P_4	6.83	0.07	1.08	1.17	0.2	--	--
P_5	4.78	0.57	0.70	0.94	--	--	--
P_6	5.01	0.04	0.90	1.01	0.5	0.6	3.94
n	6	6	6	6	5	4	4
\bar{x}	4.22	0.29	0.79	0.99	0.32	0.49	4.80
S	1.7	0.2	0.2	0.1	0.2	0.1	0.7
$t_{1-\alpha/2}$	1.48	1.48	1.48	1.48	1.53	1.64	1.64
$\bar{x} - t_{1-\alpha/2} \frac{S}{\sqrt{n}}$	3.22	0.14	0.67	0.91	0.21	0.37	4.20
$\bar{x} + t_{1-\alpha/2} \frac{S}{\sqrt{n}}$	5.22	0.44	0.91	1.08	0.43	0.60	5.39

At the failure phase, during which dry shear fracture of separating walls was observed, the joint behaviour was mapped on the basis of standard behaviours specified in PN-EN 1052-3:2004. Those tests included measurements of relative displacements of two masonry units joined with mortar and determination of fracture energy of the joint $G_f^{II} = 2.37 \cdot 10^{-4}$ MN/m [10], which could be used to describe the behaviour of the brittle material at the failure phase in accordance with the continuum fracture mechanism. The failure phase was described on the basis of observations using two sections with forces varying from N_u to N_{ag} , and then from N_{ag} to N_r at corresponding displacements u_u , u_{ag} and u_r . Assuming that fracture energy per joint area G_f^{IIj} (expressed as area below a diagram shown in Fig. 6) was equal to fracture energy G_f^{II} obtained from standard tests, the displacement corresponding to the residual force u_r was determined from the relationship:

$$AG_f^{II} = AG_f^{IIj} = \frac{1}{2}(N_u - N_{ad})(u_{ad} - u_u) + (N_{ad} - N_r)(u_{ad} - u_u) + \frac{1}{2}(N_{ad} - N_r)(u_r - u_{ad}) \Rightarrow$$

$$u_r = \frac{2G_f^{II}A - N_u(u_{ag} - u_u) + N_{ag}u_u + N_r(u_{ag} - 2u_u)}{(N_{ag} - N_r)} \quad (12)$$

Following that procedure, two values defining lower and upper limits of confidence intervals matched each of 7 coefficients (Table 5). Maximum and minimum values of displacement expressed by the relationship (12) depended from previously used values and could be considered as an independent variable. Thus, there were $\binom{7}{2}$ different combinations (without any repetitions) for coefficients. The minimum value of average square error calculated separately for forces and displacements was applied as a selection criterion. Optimal values of those coefficients were calculated from 21 combinations. A mean percent error (MPE) was calculated [16] $MPE = \frac{1}{N} \sum_{N=1}^5 \frac{x_{obs} - x_{cal}}{x_{obs}}$. The minimum MPEs for calculated forces and displacements with respect to coefficients listed in shaded cells in Table 5 were 16% (for force) and -6% (for displacement). As a result, empirical relationships based on results from model and standard tests, describing the work of joints at particular phases are presented in Table 6, and calculated values and empirically obtained values are compared in Table 7 and Fig. 5.

Table 6. Relationships describing the work of unreinforced joint between walls

Working phase of joint	Force	Stiffness	Displacement
Elastic phase	$N_{cr} = 0,67 \tau_{u,RL} A$	$K_t = 3,22 K_{RL}$	$u_{cr} = N_{cr} / 3,22 K_{RL}$
Post-elastic phase	$N_u = 0,91 \tau_{u,RL} A$	$K_p = 0,14 K_{RL}$	$u_u = (N_u - N_{cr}) / 0,14 K_{RL}$
Failure phase	$N_{ag} = 0,37 \tau_{u,RL} A$	$(N_u - N_{ag}) / (u_u - u_{ag})$	$u_{ag} = 5,39 \tau_{u,RL} A / K_{RL}$
	$N_r = 0,21 \tau_{u,RL} A$	$K_r = (N_u - N_r) / (u_r - u_u)$	$u_r = \frac{2G_f^H A - N_u(u_{ag} - u_u) + N_{ag}u_u + N_r(u_{ag} - 2u_u)}{(N_{ag} - N_r)}$

Table 7. Compared tests results and own calculations for the standard model

Test results for forces				Calculated results for forces			
$N_{cr,mv}$ kN	$N_{u,mv}$ kN	$N_{ag,mv}$ kN	$N_{r,mv}$ kN	$N_{cr,cal}$ kN	$N_{u,cal}$ kN	$N_{ag,cal}$ kN	$N_{r,cal}$ kN
39.2	50.7	24.9	16.2	33.3	46.3	19.0	10.7
Displacements				Displacements			
$u_{cr,mv}$ mm	$u_{u,mv}$ mm	$u_{ag,mv}$ mm	$u_{r,mv}$ mm	$u_{cr,cal}$ mm	$u_{u,cal}$ mm	$u_{ag,cal}$ mm	$u_{r,cal}$ mm
0.09	0.243	2.08	5.58	0.09	0.24	2.34	6.53

In accordance with assumptions Calculated forces determining coordinates for particular phases of joint work were weaker than those obtained from tests which was consistent with assumptions. Considering the force causing cracks, the difference was 15%, and for the failure force – 9%. The biggest differences were found at the failure phase. Then, calculated values N_{ag} and N_r were lower by 36% and 44% than average empirical values. For relative displacement at the elastic phase, the calculated displacement differed from the average empirical value by only 3%, and by 7% in case of the greatest force. At the failure phase, displacements corresponding to forces N_{ag} and N_r differed by 12% and 17%, respectively. Delivered results were sufficient to predict forces with the satisfactory precision, and thus to verify properly SLS conditions for joints. Greater differences were found for displacements, which are crucial for verifying SLS conditions. And the biggest discrepancy was obtained for the maximum load.

3.2. Reinforced models

In models of series **B10** and **BP10** reinforced with steel connectors no cracks on walls typical for unreinforced models were observed for the whole range of loading. Displacements of interconnected wall panels were unnoticeable at the initial phase of loading. At a given moment a rapid increase in displacements was clearly visible to the naked eye. But it was still possible to continue loading of models until the time of destruction. The destruction was rapid and caused shearing of the joint and a distinct vertical displacement (by ca. 17 mm) of the wall web – Fig. 7b. The wall settled on the wooden protection. Models at the failure are shown in Fig. 7a. Destruction of models of series **B10** and **BP10** was caused by destroyed by plastification and bending of steel flat bars in the vicinity of the contact surface (Figs 7c and 7d). Spalling of masonry units below each connector was observed at the wall edge (see arrows in Figs 7c, d). The measured length of spalling areas was ca. 15 mm. However, no shear fracture of the connector was observed in mortar laid in bed joints due to holes in the flat bar. Mortar penetrating through holes was not subjected to shearing. It acted as a dowel and prevented displacement. For **B10** models, an increase in displacements was observed at lower values of the loading force when compared to **BP10** models.

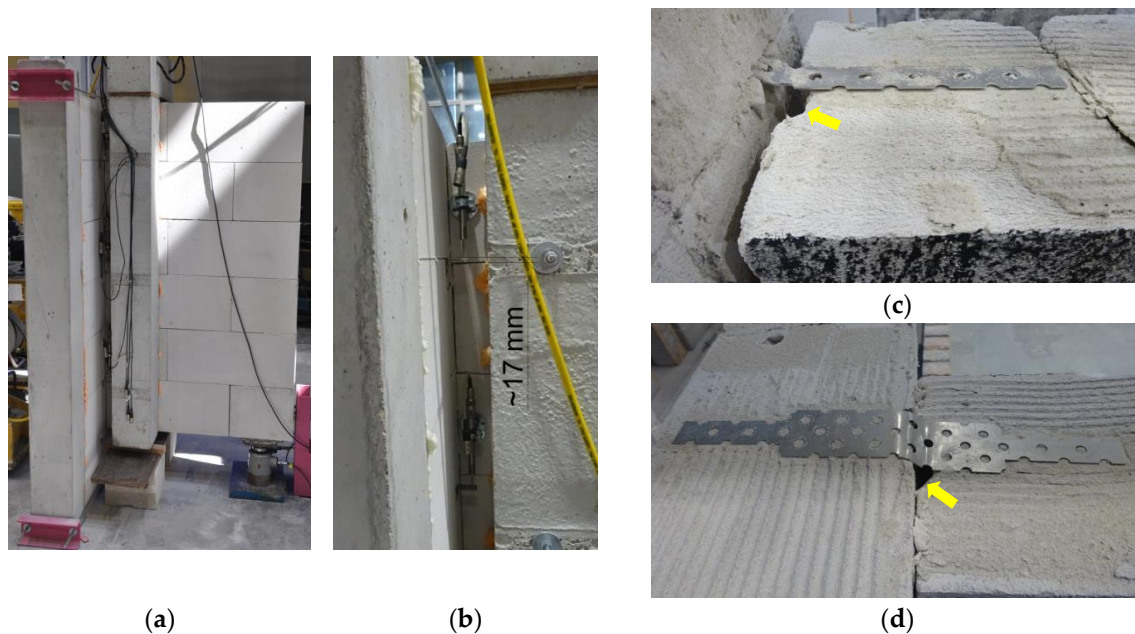


Figure 7. Destruction of reinforced models: a) damaged mode (B10_1), b) damaged model with dimensioned displacement between bed joints (B10_2), c) typical bending of punched flat bar near the contact surface (B10_1), d) typical bending of punched flat bar near the contact surface (BP10_3)

Bent connectors were removed from crumbled models, inspected and their permanent deformation was evaluated – Fig. 8. The shape of connectors was original - straight, in areas of anchoring in joints. However, the permanent deformation occurred in the central area where connectors crossed wall joints. A permanent displacement u_u perpendicular to the connector axis was observed in the section marked e_u . Additionally, the representative total extension of each connector δ_u was calculated. A permanent displacement e_u in models B10 ranged from 20 mm to 27 mm, and the average was 23 mm (23t) at the average displacement u_u between 8 mm and 17 mm and the average of 11 mm (11t). A permanent displacement e_u in models BP10 ranged from 20 mm to 29 mm, and the average was 23 mm (23t). The vertical displacement u_u was between 8 mm and 17 mm, and the average was 12 mm (12t). Deformation seemed to be identical despite the shape of connectors. The only reported difference was the position of the deformed area regarding the mid-length of the connector. Displacements observed for some connectors were of the order of ± 20 mm regarding the mid-length of the connector. As no regularity caused by e.g. their position in joints was found, the above was assumed to be the effect of precisely made joints. Measured geometry of connectors in each model and average values are presented in Table 8.

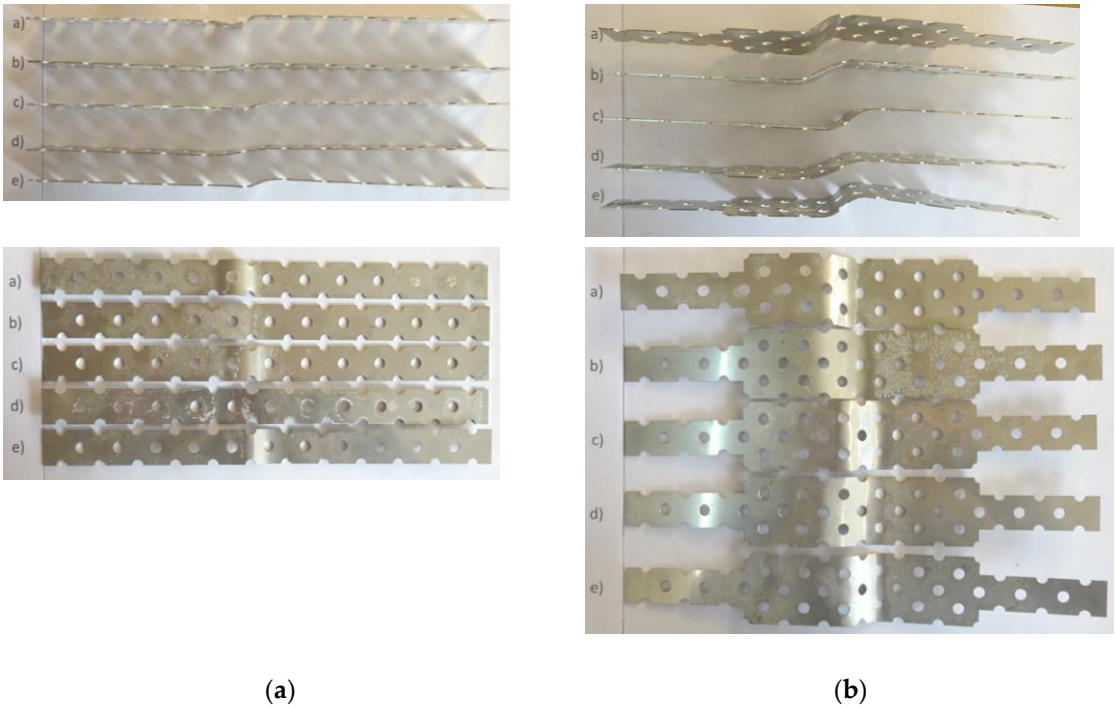
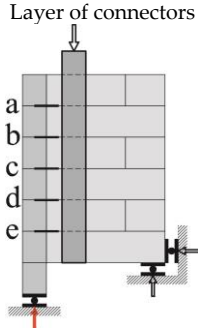
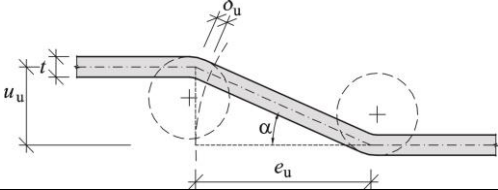


Figure 8. Deformed connectors removed destroyed research models after tests: a) punched flat bars in the wall B10_2, b) punched expanded flat bars in the wall BP10_2

Table 8. Measured geometry of deformed connectors

Model							
		distance between points of contraflexure		relative displacement of connector ends		connector extension of	
		$e_{u,i}$ mm	$e_{u,mv}$ mm	$u_{u,i}$ mm	$u_{u,mv}$ mm	$\delta_{u,i} = \sqrt{e_{u,i}^2 + u_{u,i}^2} - e_u$ mm	$\delta_{u,mv}$ mm
1	2	3	4	5	6	7	8
B10_1	a	23	22	9	9	1.70	1.8
	b	21		8		1.47	
	c	20		9		1.93	
	d	24		9		1.63	
	d	21		10		2.26	
B10_2	a	26	24	11	10	2.23	2.2
	b	26		10		1.86	
	c	25		11		2.31	
	d	22		10		2.17	
	d	20		10		2.36	

Cont. table 8. Measured geometry of deformed connectors

1	2	3	4	5	6	7	8
B10_3	a	21		11		2.71	
	b	23		13		3.42	
	c	23	23	15	14	4.46	3.7
	d	23		12		2.94	
	d	27		17		4.91	
			23 (23t)	--	11 (11t)	--	2.57 (2.57t)
BP10_1	a	19		12		3.47	
	b	27		14		3.41	
	c	24	24	13	13	3.29	3.33
	d	29		11		2.02	
	d	23		15		4.46	
BP10_2	a	23		17		5.60	
	b	22		14		4.08	
	c	27	23	14	15	3.41	4.22
	d	22		13		3.55	
	d	23		15		4.46	
BP10_3	a	22		12		3.06	
	b	23		10		2.08	
	c	19	23	9	10	2.02	2.01
	d	26		8		1.20	
	d	23		9		1.70	
			23 (23t)	--	13 (13t)	--	3.28 (2.57t)

As in case of unreinforced joints, phases of reinforced joints can be presented in diagrams illustrating the relationship between the load N and relative (mutual) displacement u of bonded walls – Fig. 9.

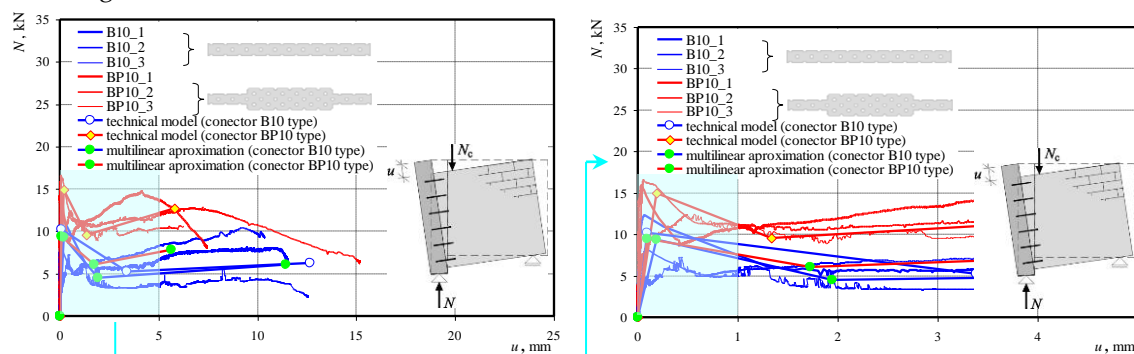


Figure 9. Relationship between the total force and average displacement of joint

Until the crack on the contact area that appeared under the maximum load $N_{cr} = N_u = 7.3 - 12.3$ kN for models **B10** and $12.5 - 16.5$ kN for models **BP10**, an increment in displacement was nearly proportional and that phase was defined as the elastic phase. A clear increase in displacements and a drop in force to $N_d = 3.4 - 5.0$ kN in models **B10** and $8.9 - 10.5$ kN in models **BP10** was observed after cracking at the failure phase. When the force N_d was achieved at the failure phase, the joint demonstrated the power to take load, and small reinforcement was noticed. Destruction of models

caused by excessive displacements was observed under the maximum load $N_{cr} = N_u = 2.3 - 9.2$ kN for models **B10** and $10.6 - 14.8$ kN for models **BP10**. Thus, a drop in the residual force of the maximum force was ca. 35% for models **B10** and only 15% for models **BP10**. Connectors **B10** produced lower values of the force at individual working phases. Loading at the time of cracking was lower by 76%, and the maximum loading was lower by as much as 82%. Also, the residual force was lower by 63% when compared to the force determined for unreinforced models. Displacements in the reinforced models at the greatest force were lower only by 18% than in the unreinforced joint. Displacements in reinforced joints greater than 100% were found under the residual force at the end of the failure phase. When compared to unreinforced models, the cracking force acting on models with connectors **BP10** with a broadened central part was lower by 62% than in the model with the traditional joint. The maximum cracking force acting on reinforced models was lower by 71% than in case unreinforced models. Also the residual force was greater by more than 63%. Displacements in the reinforced models at the greatest force were lower by 15% than in the unreinforced joint. And displacements slightly greater by 4% than in unreinforced models were observed under the residual force at the end of the failure phase. A twofold broadening of the connector in models **BP10** resulted in ca. 60% increase of forces N_u and over 100% increase in forces N_d and N_r when compared to results obtained for models **B10**. Displacements in models with a wider connectors were as expected almost identical at the elastic phase and lower by 30-50% at the failure phase. Observed phases were the base for a multi-sectional diagram illustrating the $N - u$ relationship for working joints in AAC walls – Fig.10. The elastic phase was defined within the loading range $0 - N_{cr}=N_u$, and the failure phase within the range $N_u - N_d - N_r$.

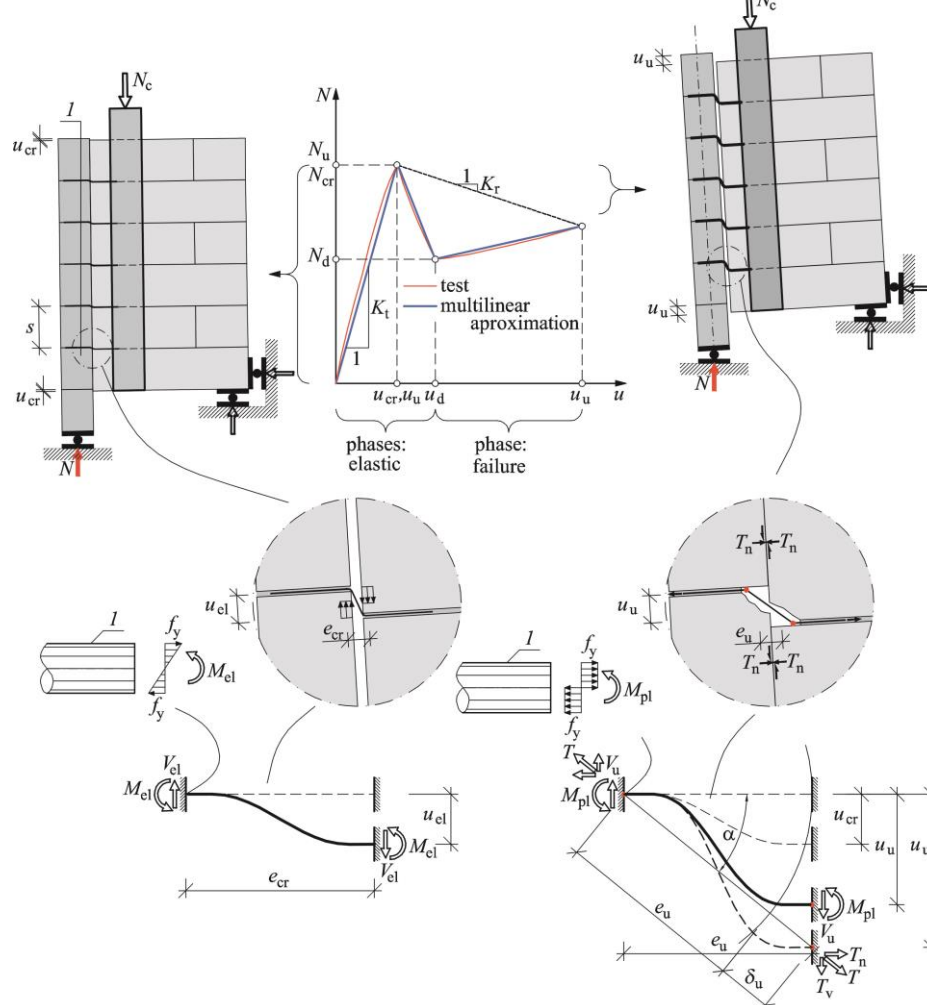


Figure 10. Approximation of work of reinforced joint between masonry walls (1 – connector)

Values of forces and corresponding displacements are presented in Tables 9 and 10. Joint stiffness was determined in each working phase according to equations (1) – (3) and they are presented in Table 11. A linear approximation of results is shown in Fig. 10.

Table 9. Test results for reinforced joints – forces

Model	Cracking force		Force at failure		Dowel force		Residual force	
	$N_{cr,i}$	$N_{cr,mv}$	$N_{u,i}$	$N_{u,mv}$	N_d	$N_{d,mv,i}$	$N_{r,i}$	$N_{r,mv}$
	kN	kN	kN	kN	kN	kN	kN	kN
B10_1	12.3		12.3		5.01		6.68	
B10_2	8.41	9.3	8.41	9.3	5.02	4.5	9.20	6.1
B10_3	7.27		7.27		3.39		2.32	
BP10_1	15.9		15.9		8.86		14.8	
BP10_2	16.5	14.9	16.5	14.9	10.5	9.6	12.6	12.7
BP10_3	12.4		12.4		9.36		10.6	

Table 10. Test results for reinforced joints – displacements

Model	Displacement at the time of cracking		Displacement right before failure		Displacement at dowel force		Residual displacement	
	$U_{cr,i}$	$U_{cr,mv}$	$U_{u,i}$	$U_{u,mv}$	$U_{d,i}$	$U_{d,mv}$	$U_{r,i}$	$U_{r,mv}$
	mm	mm	mm	mm	mm	mm	mm	mm
B10_1	0.07		0.07		1.83		11.50	
B10_2	0.08	0.19	0.08	0.19	0.68	1.94	10.33	11.45
B10_3	0.41		0.41		3.32		12.52	
BP10_1	0.04		0.04		0.45		4.15	
BP10_2	0.05	0.19	0.05	0.19	1.61	1.33	7.04	5.80
BP10_3	0.49		0.49		1.94		6.22	

Table 11. Test results for reinforced joints - stiffness

Model	Elastic joint stiffness		Residual joint stiffness	
	$K_{t,i}$	$K_{t,mv}$	$K_{r,i}$	$K_{r,mv}$
	MN/m	MN/m	MN/m	MN/m
B10_1	180		0.496	
B10_2	102	100	0.077	0.327
B10_3	17.8		0.409	
BP10_1	432		0.269	
BP10_2	319	259	0.553	0.378
BP10_3	25.6		0.312	

3.2.1. Validation of the model representing reinforced joints in walls

Like for unreinforced joints, the obtained results were generalised. The following assumptions were made:

- d) a non-linear relationship $N - u$ determined from tests was replaced with a multi-sectional relationship expressing all observed working phases:
 - i. the elastic phase observed in the load range $0 - N_{cr} = N_u$,
 - i. the failure phase observed in the load range $N_u - N_d - N_r$,

- e) all material parameters used in the model were suggested to be specified in standard and normalised methods,
- f) an elastic - perfectly plastic model of the connector was used,
- g) the model would be subjected to statistical validation on the basis of performed tests.

The behaviour of joint was described with simplified solutions found in the literature [11, 12]. According to cited papers, connectors were working as bars fixed on both sides, and the value of force causing the displacement u could be expressed as follows:

$$V = \frac{12E_s I}{e^3} u, \quad (13)$$

a corresponding bending moment in the connector is equal to:

$$M = \frac{6E_s I}{e^2} u, \quad (14)$$

where: EI – flexural stiffness of connector, u – relative displacement of connector ends, e – representative length of connector (distance between points of contraflexure).

Stress values of terminal fibres in the connector fixed in bed joints were increasing proportionally to the displacement u . For some displacements u_{el} , stress at terminal fibres reached the yield point, and the bending moment and the shearing force were expressed by following equations:

$$M_{el} = f_y W_{el} = \frac{6E_s I}{e_{el}^2} u_{el}, \quad V_{el} = \frac{2M_{el}}{e_{el}}. \quad (15)$$

where: W_{el} – elastic indicator of transverse bending of connector section, f_y – representative yield point of steel in connector, e_{el} – connector length at the elastic phase.

An increase in relative displacements of ends of connectors was observed with the plastification of the total section of the connector resulting the highest bending moment and the greatest shearing force equal to:

$$M_{pl} = f_y W_{pl} = \frac{6E_s I}{e_{pl}^2} u_{pl}, \quad V_u = \frac{2M_{pl}}{e_{pl}}, \quad (16)$$

where: W_{pl} – plastic indicator of transverse bending of connector section, f_y – representative yield point of steel in connector, e_{pl} – connector length at the plastic phase.

An increase in relative displacements could cause spalling of the wall under the connector and an increase in the length of connectors. That, in turn, could produce a noticeable drop of force in joints. As in previous phases, bending moments in connectors and shearing forces were determined from the following relationship:

$$M_d = f_y W_{pl} = \frac{6E_s I}{e_d^2} u_d, \quad V_d = \frac{2M_d}{e_d}, \quad (17)$$

Tests demonstrated that further increase in relative displacements could cause an increase of forces in joints. At that working phase, displacements were so considerable that connectors could work in a flexible and also tendon mode. Consequently, friction force was generated between joined walls. The bending moment and shearing forces in the joint can be expressed as:

$$M_u = f_y W_{pl} = \frac{6E_s I}{e_u^2} u_u, \quad V_u = \frac{2M_u}{e_u}, \quad (18)$$

And the axial force in the joint induced by tendon work was:

$$T = E_s A \frac{\delta_u}{e_u}, \quad (19)$$

where: δ_u – extension of connector determined from the equation:

$$\delta_u = \sqrt{e_u^2 + u_u^2} - e_u. \quad (20)$$

Horizontal and vertical components of force, being the effect of the tendon work (at $\alpha \approx 0$) were equal to:

$$\begin{aligned} T_n &= T \cos \alpha \approx T, \\ T_v &= T \sin \alpha \approx 0. \end{aligned} \quad (21)$$

Taking into account the tendon work of connectors, the load capacity of reinforced joints in walls can be expressed as:

$$V_u = \frac{2f_y W_{pl}}{e_u} n_c + \alpha n_c E_s A \frac{\delta_u}{e_u} \mu, \quad (22)$$

where: μ – friction coefficient, α – empirical coefficient, e_u – average length of connector (distance between points of contraflexure acc. to Table 8), $n_c = 5$ – number of connectors.

The corresponding displacement is expressed by the following relationship:

$$u_u = \frac{f_y W_{pl} e_u^2}{6E_s I} \beta \quad (23)$$

where: μ – friction coefficient, β – empirical coefficient.

Forces at the failure phase can be determined similarly.

$$V_d = \frac{2f_y W_{pl}}{e_u} n_c + \alpha_1 n_c E_s A \frac{\delta_u}{e_u} \mu, \quad (24)$$

$$u_d = \frac{f_y W_{pl} e_u^2}{6E_s I} \beta_1 \quad (25)$$

$$V_r = \frac{2f_y W_{pl}}{e_u} n_c + \alpha_2 n_c E_s A \frac{\delta_u}{e_u} \mu, \quad (26)$$

$$u_r = \frac{f_y W_{pl} e_u^2}{6E_s I} \beta_2 \quad (27)$$

Above equations included not only mechanical parameters of connectors (E , f_y) but also the measured length of connectors e_u – distance between points of contraflexure. However, that approach is not unconditional. Length of connectors measured in own tests was ca. $23t$. The paper [11] determined experimentally that the length of connectors from flat bars was $(1.6 - 2.5)t$ provided that masonry units below the connector were not crushed as observed in models made of AAC. Like for unreinforced models, values of empirical coefficients were calculated using results from material tests and test on individual elements. Boundary values of average coefficients α , α_1 , α_2 , β , β_1 , β_2 were determined at the significance level $\alpha = 0.8$. As the sample size was small, the relationship expressed by the relationship (11) was used. Lower and upper values from the confidence interval of average coefficients are presented in Table 12.

Table 12. Validation of empirical coefficients of the model with reinforced wall joints

Model	x_i					
	$\alpha_i = \frac{V_{u,i} - \frac{2f_y W_{pl}}{e_u} n_c}{n_c E_s A \frac{\delta_u}{e_u} \mu}$	$\beta_i = \frac{6E_s I u_{u,i}}{f_y W_{pl} e_u^2}$	$\alpha 1_i = \frac{V_{d,i} - \frac{2f_y W_{pl}}{e_u} n_c}{n_c E_s A \frac{\delta_u}{e_u} \mu}$	$\beta 1_i = \frac{6E_s I u_{d,i}}{f_y W_{pl} e_u^2}$	$\alpha 2_i = \frac{V_{r,i} - \frac{2f_y W_{pl}}{e_u} n_c}{n_c E_s A \frac{\delta_u}{e_u} \mu}$	$\beta 2_i = \frac{6E_s I u_{r,i}}{f_y W_{pl} e_u^2}$
B10_1	0.01117	0.10	0.00421	2.73	0.00580	17.2
B10_2	0.00744	0.12	0.00422	1.02	0.00819	15.4
B10_3	0.00636	--	0.00268	--	--	18.7
n	3	2	3	2	2	3
\bar{x}	0.00832	0.11	0.003702	1.88	0.00699	17.11
S	0.00253	0.0146	0.0008880	1.21	0.00169	1.63
$t_{1-\alpha/2}$	1.89	3.08	1.89	3.08	3.08	1.89
$\bar{x} - t_{1-\alpha/2} \frac{S}{\sqrt{n}}$	0.00557	0.081	0.00274	-0.75	0.0033	15.33
$\bar{x} + t_{1-\alpha/2} \frac{S}{\sqrt{n}}$	0.01107	0.145	0.00467	4.50	0.0107	18.89
BP10_1	0.00619	0.06	0.00328		0.00573	
BP10_2	0.00645	0.08	0.00397	2.43	0.00484	10.6
BP10_3	0.00476		0.00348	2.91	0.00401	9.4
n	3	2	3	2	3	2
\bar{x}	0.00580	0.07	0.00358	2.67	0.00486	9.98
S	0.000911	0.0	0.000356	0.3	0.000859	0.877
$t_{1-\alpha/2}$	1.89	3.08	1.89	3.08	1.89	3.08
$\bar{x} - t_{1-\alpha/2} \frac{S}{\sqrt{n}}$	0.0048	0.0319	0.00319	1.93	0.0039	8.1
$\bar{x} + t_{1-\alpha/2} \frac{S}{\sqrt{n}}$	0.0068	0.1014	0.0040	3.41	0.0058	11.9

Following the procedure conducted for unreinforced joints, two values defining lower and upper limits of confidence intervals matched each of 6 coefficients (Table 12). Thus, there were $\binom{6}{2}$ different combinations (without any repetitions) for coefficients. Similarly as for unreinforced joints, the minimum value of mean percentage error (MPE) [16] was applied as a selection criterion separately for forces and displacements. Optimal values of those coefficients were calculated from 15 combinations. Optimal values of those coefficients were calculated from 15 combinations. For values of coefficients in shaded cells in Table 12, the minimum MPE for forces and displacements in connectors B10 was equal to 22%. For connectors BP10, MPE for forces and displacements was 11%. Using results from model and standard tests, empirical relationships describing the work of joints at particular phases are presented in Table 13, and calculated values and empirically obtained values are compared in Table 14 and Fig. 10.

Table 13. Relationships expressing the work of reinforced joints in walls -

Working phase of joint	Force	Stiffness	Displacement
Connector B10			
Elastic phase	$V_u = \frac{2f_y W_{pl}}{e_u} n_c + 0,0056 E_s A \frac{\delta_u}{e_u} \mu$	$K_t = V_u / u_u$	$u_u = 0,145 \frac{f_y W_{pl} e_u^2}{6 E_s I}$
Failure phase	$V_d = \frac{2f_y W_{pl}}{e_u} n_c + 0,0027 E_s A \frac{\delta_u}{e_u} \mu$	$K_r = (V_u - V_r) / (u_r - u_u)$	$u_d = 4,50 \frac{f_y W_{pl} e_u^2}{6 E_s I}$
	$V_r = \frac{2f_y W_{pl}}{e_u} n_c + 0,0023 E_s A \frac{\delta_u}{e_u} \mu$		$u_r = 18,9 \frac{f_y W_{pl} e_u^2}{6 E_s I}$
Connector BP10			
Elastic phase	$V_u = \frac{2f_y W_{pl}}{e_u} n_c + 0,0048 E_s A \frac{\delta_u}{e_u} \mu$	$K_t = V_u / u_u$	$u_u = 0,10 \frac{f_y W_{pl} e_u^2}{6 E_s I}$
Failure phase	$V_d = \frac{2f_y W_{pl}}{e_u} n_c + 0,0032 E_s A \frac{\delta_u}{e_u} \mu$	$K_r = (V_u - V_r) / (u_r - u_u)$	$u_d = 1,93 \frac{f_y W_{pl} e_u^2}{6 E_s I}$
	$V_r = \frac{2f_y W_{pl}}{e_u} n_c + 0,0039 E_s A \frac{\delta_u}{e_u} \mu$		$u_r = 8,1 \frac{f_y W_{pl} e_u^2}{6 E_s I}$

Table 14. Compared tests results and own calculations for the standard model

Test results for connector B10			Test results for connector B10		
forces			forces		
$N_{cr,mv} = N_{u,mv}$	$N_{d,mv}$	$N_{r,mv}$	$N_{cr,cal} = N_{u,cal}$	$N_{d,cal}$	$N_{r,cal}$
kN	kN	kN	kN	kN	kN
9.34	4.47	6.07	6.44	3.45	4.06
Displacements of connector B10			Displacements of connector B10		
$U_{cr,mv} = U_{u,mv}$	$U_{ag,mv}$	$U_{r,mv}$	$U_{cr,cal} = U_{u,cal}$	$U_{u,cal}$	$U_{r,cal}$
mm	mm	mm	mm	mm	mm
0.19	1.94	11.45	0.10	3.01	12.6
Test results for connector BP10			Test results for connector BP10		
force			force		
$N_{cr,mv} = N_{u,mv}$	$N_{d,mv}$	$N_{r,mv}$	$N_{cr,cal} = N_{u,cal}$	$N_{d,cal}$	$N_{r,cal}$
kN	kN	kN	kN	kN	kN
14.94	9.59	12.69	12.6	8.65	10.43
Displacements of connector BP10			Displacements of connector BP10		
$U_{cr,mv} = U_{u,mv}$	$U_{ag,mv}$	$U_{r,mv}$	$U_{cr,cal} = U_{u,cal}$	$U_{u,cal}$	$U_{r,cal}$
mm	mm	mm	mm	mm	mm
0.19	1.33	5.80	0.07	1.29	5.40

For standard connectors **B10** without broadening, calculated forces determining coordinates of particular work phases were lower than those obtained during tests. The difference for the maximum force was equal to 31%, and for the aggregate interlocking force – 23%. The value of the force N_r at the failure phase was lower by 33% than the empirical value. Similar results were obtained for connectors **BP10**. Determined force values were lower than experimental ones. The maximum force N_u was lower by 16%, and forces V_d and V_r at the failure phase were lower by 10% and 18% respectively when compared to forces determined experimentally. Calculated displacements of joints with connectors **B10** significantly varied. The calculated displacement at failure was lower by 48% than experimentally determined values. And displacements at the failure

phase corresponding to the force V_d were greater by over 55% than experimental values, and calculated displacements were greater only by 10%. For connectors **BP10**, displacements at the maximum force were underestimated at the level of over 65%, and overestimated by only 3% under the force V_d . Differences in calculated and measured displacements at failure were equal to just 7%. Obtained results, particularly for forces, can be used to estimate with the safe margin forces in joints and to verify SLS conditions where no guidelines can be applied. Similarly as for unreinforced joints, the greatest differences were observed for displacements. The recommended relationships can cause a significant underestimation of displacement at failure, even at the level of ca. 50%.

4. Conclusions

Tests described in this paper are a part of complex research works conducted by the Silesian University of Technology. This paper presents results from testing three types of wall joints: a traditional mortar bonding (URM), joints with punched steel flat bars (**B10**) and with connectors of genuine shape (**BP10**) protected by patent.

The destruction process and crack development on the wall bonded with mortar were mild and included three phases. Distinct wall cracks near the joint were observed prior to failure. Destruction and cracking of models with steel elements, apart from lower load capacity, were completely different. No cracks preceding the wall destruction were observed, but there were rapid displacements and a drop in loading. For perforated flat bars used as steel connectors, significantly lower values were obtained when compared to models with mortar bonding. Forces at the time of cracking were lower by 62% (**BP10**) – 76% (**B10**), and the difference at the maximum force was 82% (**BP10**) – 71% (**B10**). Reinforced models were less deformed at the elastic phase. Differences at the maximum force were 18% (**B10**) and 15% (**BP10**). Greater differences were observed for displacements prior to the failure. Displacements in models with reinforced joints **B10** were greater by over 100% than in unreinforced models. Generally the same displacements were reported for models with connectors **BP10**. A twofold broadening of the connector in models **BP10** resulted in ca. 60% increase of maximum forces when compared to results obtained for models **B10**. Displacements in models with a wider connectors were as expected almost identical at the elastic phase and lower by 30-50% at the failure phase.

Individual working phases of joints were determined and defined, and the empirical approach was suggested to determine forces and displacement of wall joints using results from less complicated standard tests. Values of cracking and failure forces were estimated with a safety margin for unreinforced joints. And they differed by 15% and 9% in comparison to test results. On the basis of relationships described in the literature, a technical solution was proposed, which included the determination of forces producing cracks on the contact area and maximum forces in joints between walls reinforced with perforated steel flat bars. Due to small number of elements per series, differences in safe estimation of forces were of the order of 31% for maximum forces in connector **B10**, and 26% in connector **BP10**.

Works should be continued and additional research models should be developed to statistically define empirical parameters of models. Then, results of validation are expected to provide lower differences in extreme values. Also FEM analyses seem to be necessary to determine the real work joints, particularly to determine their real length – e. The target model should also give consideration to the phase of joint weakening and to estimation of forces N_{cr} , N_d and N_u and corresponding displacements at the satisfactory accuracy.

Acknowledgements: The authors would like to express particular thanks to Solbet Sp. z o.o. and NOVA Sp. z o.o. companies for valuable suggestions and delivery of masonry units, mortar, and connectors which were used to prepare research models and perform tests.

Author Contributions: Conceptualization, R.J. and I.G.; methodology, R.J. and I.G; validation, R.J.; formal analysis, I.G; investigation, I.G; writing—original draft preparation, R.J.; writing—review and editing, I.G; visualization, R.J. and I.G.; supervision, R.J and I.G.

Conflicts of Interest: The authors declare no conflict of interest.

References

1. **Galman, Iwona, Jasiński, Radosław**, Joints in masonry walls. 6th International Conference on Autoclaved Aerated Concrete. September 4 – 3, 2018, University Postam.
2. **Galman Iwona, Jasiński, Radosław**, *Tests of joints in AAC masonry walls*. Architecture Civil Engineering Environment, 2018 vol. 11 no 4, pp. 79 – 92. DOI: 10.21307/ACEE-2018-056.
3. **PN-EN 1052-1:2000** Methods of tests for masonry. Part 1: Determination of Compression Strength. (In Polish).
4. **Jasiński, Radosław, Drobiec, Łukasz**, Comparison Research of Bed Joints Construction and Bed Joints Reinforcement on Shear Parameters of AAC Masonry Walls. Journal of Civil Engineering and Architecture, Vol. 10, 12/2016, pp. 1329 – 1343. DOI: 10.17265/1934-7359/2016.12.004.
5. **PN-EN 1052-3:2004** Methods of tests for masonry. Part 3: Determination of Initial Shear Strength. (In Polish)
6. **Drobiec, Łukasz, Jasiński, Radosław**, Influence of the kind of mortar on mechanical parameters of AAC masonry subjected to shear – the basic strength parameters. Materiały Budowlane 5/2015, pp. 106 – 109, 2015. DOI: 10.15199/33.2015.05.44. (in Polish).
7. **ASTM E519-81** Standard Test Method for Diagonal Tension (Shear) of Masonry Assemblages.
8. **Drobiec, Łukasz, Jasiński, Radosław**, Influence of the kind of mortar on mechanical parameters of AAC masonry subjected to shear – dilatational deformability. Materiały Budowlane 7/2015, pp. 116 – 119. DOI: 10.15199/33.2015.07.32. (in Polish).
9. **Galman, Iwona, Jasiński, Radosław**, *Attempt to Describe the Mechanism of Work of Masonry Joints*”. IOP Conf. Series: Materials Science and Engineering 471 (2019) 052054. doi:10.1088/1757-899X/471/5/052054.
10. **Jasiński, Radosław**, Research and modeling of masonry shear walls, PhD DsC Thesis. Silesian University of Technology, Gliwice, Poland 2017. (In Polish)
11. **Simudic, G., Page, A., W.**, Australian developments in the use of walls of geometric section, 7th North American Masonry Conference. University of Notre Dame-South Bend, Indiana, USA 2-5 June 1996. Vol. 2, pp. 1007-1018.
12. **Phipps, M., E., Montague, T., I.**, The behaviour and design of steel shear connectors in plain and prestressed masonry, 7th North American Masonry Conference. University of Notre Dame-South Bend, Indiana, USA 2-5 June 1996. Vol. 2, pp. 789-798.
13. **PN-EN 10002-1:2004** Metallic materials - tensile testing. Part 1. Method of test at ambient temperature.
14. **Volk, William**, *Applied Statistics for Engineers*. Literary Licensing, LLC, United States, 2013.
15. Polish Patent Office, ul. Niepodległości 188/192, 00-950 Warsaw (Poland). Application from 2019/04/01 No. W.128153. Wall joint connector.
16. **Freedman, David, Pisani, Robert, Purves, Roger**, Statistics. Publisher: W.W. Norton & Company; 4th edition (February 13, 2007).